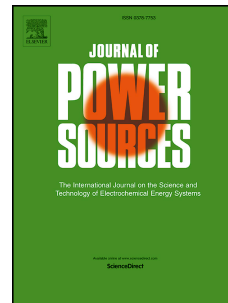# Accepted Manuscript

The contribution of sulfate ions and protons to the specific capacitance of microporous carbon monoliths

V. Barranco, A. Garcia-Gomez, M. Kunowsky, A. Linares-Solano, J. Ibañez, M. King, J.M. Rojo

The contribution of sulfate ions and protons to the specific capacitance of microporous carbon monoliths.

V. Barranco[1], A. Garcia-Gomez[1], M. Kunowsky[2], A. Linares-Solano[2], J. Ibañez[3], M. King[4], and J.M. Rojo[1]*

1. Instituto de Ciencia de Materiales de Madrid, ICMM; CSIC; Sor Juana Ines de la Cruz, 3; Cantoblanco; 28049-Madrid; Spain.

2. Grupo MCMA; Departamento de Quimica Inorganica; Universidad de Alicante; Ap. 99; 03080-Alicante; Spain.

3. Centro Nacional de Investigaciones Metalurgicas, CENIM; CSIC; 28040-Madrid; Spain

4. ATMI, Adsorbent and Gas Technology; Danbury; Connecticut 06810; USA.

*corresponding author: jmrojo@icmm.csic.es

Abstract

The monoliths studied in this work show large specific surface areas (up to 1600 m^2 g^{-1}), high densities (up to 1.17 g cm^{-3}) and high electrical conductivities (up to 9.5 S cm^{-1}). They are microporous carbons with pore sizes up to 1.3 nm but most of them below 0.75 nm. They also show oxygen functionalities. The electrochemical behavior of the monoliths is studied in three-electrode cells with aqueous H_2SO_4 solution as electrolyte. This work deals with the contribution of the sulfate ions and protons to the specific capacitance of carbon monoliths having different surface areas and different contents of oxygen groups. Protons contribute with a pseudocapacitance (up to 152 F g^{-1}) in addition to the double layer capacitance. Sulfate ions contribute with a double layer capacitance only. At the double layer, the capacitance of the sulfate ions (up to 291 F g^{-1}) is slightly higher than that of protons (up to 251 F g^{-1}); both capacitances increase as the surface area increases. The preference of protons to be electroadsorbed at the double layer and the broader voltage window of these ions account for their higher contribution (70 %) to the double layer capacitance.

Key words: carbon monolith; microporous carbon; sulfuric acid electrolyte; supercapacitor; EDLC.

1. Introduction

Carbon monoliths consist of a three-dimensional network of linked carbon particles [1-5]. They show higher electrical conductivity compared to compacted powder pellets, as a consequence of the better contact between adjacent particles [6]. Carbon monoliths usually show a hierarchical porosity derived from the connectivity of macro/mesopores and micropores [1-6]. Both hierarchical porosity and high electrical conductivity account for the application of carbon monoliths as supercapacitor electrodes.

Although carbon monoliths have been prepared before [1,2,7-17], only in the last few years have they been studied as electrodes in their current form, i.e. as an entire piece of carbon [6,18-32]. Cells having carbon monoliths as electrodes have a number of advantages over those comprising compacted powder pellets made from powder carbon. Indeed, the cells with monolithic electrodes reach higher capacitances, lower electrical resistances and shorter response times (i.e. faster charge/discharge of the cell) [6]. The effect of the three-dimensional character of the monolith on the electrical response of the cells has also been studied [21]. As the monolith height increases, (i) the cell capacitance increases significantly, which is an advantage, (ii) the cell resistance increases slightly, which is a moderate drawback, and (iii) the response time becomes longer, which is an important drawback. So, thicker monoliths are better for improving cell energy and thinner monoliths are better for improving cell power [21,22].

Like other carbons, the carbon monoliths can be doped with heteroatoms (oxygen, nitrogen, phosphorus, sulfur,…), the doping giving rise to an increase of the specific capacitance or to a broadening of the working voltage window [33-38]. The high electrical conductivity makes carbon monoliths suitable substrates for depositing other active electrode materials such as polymers [39] or oxides [40,41]. In general, the

3

carbon monoliths are isotropic materials; however, some monoliths are anisotropic and show carbon walls and channels, both aligned along a specific direction of the monolith [21]. The main drawback of the carbon monoliths is their low density, typically lower than 0.5-0.6 g cm^{-3} [2,20-32]. Consequently, their volumetric capacitance is usually low, below 100 F cm^{-3} in aqueous electrolytes and below 50 F cm^{-3} in organic ones.

The usual procedures to prepare porous carbon monoliths are: (i) From carbonization of gels obtained from several carbon precursors and catalysts [1,2,11-15,18, 24,25, 29,31], (ii) From carbonization of gels having a "template" that is removed either thermally during carbonization, or chemically by reaction with specific reagents [4,8,23], (iii) From infiltration of an inorganic monolith with a carbon precursor followed by carbonization of the precursor and removal of the inorganic template [8,9,13,30], (iv) From carbonization of a natural monolith, e.g. a piece of wood or of bone [28,32], and (v) From mold conforming (with or without binder) under pressure of several carbon or carbon precursors followed by carbonization [20,21,26,27]. A modification of the latter case includes carbonization of a carbon precursor, e.g. polyvinylidenechloride (PVDC)-based copolymers, as produced by ATMI, Inc (BrightBlack® carbon monolith).

The ATMI carbon monolith, which is the starting carbon monolith studied in this work, is a microporous carbon that combines high density (1.17 g cm^{-3}), large specific surface area (ca. 1000 m^2 g^{-1}) and high electrical conductivity (9.3 S cm^{-1}). These characteristics account for a high gravimetric capacitance (292 F g^{-1}) and volumetric one (342 F cm^{-3}) and a high capacitance retention on current as measured in sulfuric acid as electrolyte [42]. This work, which shows the highest volumetric capacitance ever reported in acidic electrolyte, was made from electrochemical measurements in two-electrode cells. Hence, the capacitances reported came from the contribution of the two types of ions, sulfate ions and protons, and these contributions were unknown. The aim of the present work is to analyze and understand the contribution of the two ions to the specific capacitance of monoliths having different surface chemistries and

4

porosities. The pseudo capacitance is analyzed for each ion and discussed in relation to the content of oxygen groups at the surface of the monoliths. The double layer capacitance is discussed in terms of the double layer capacitance of each ion, and these capacitances are related to the surface areas and porosities of the monoliths. The amount of each electroadsorbed ion at the double layer is assessed. The voltage window of each ion is measured and discussed in relation to the total voltage window of a real supercapacitor.

2. Experimental

Carbon monoliths were produced by pyrolysis of PVDC copolymers by ATMI Inc. They are commercially available (BrightBlack®) as cylindrical pieces of 9 cm in diameter and 2 cm in height. From these pieces, smaller monoliths, also of cylindrical shape, were extracted. These monoliths, here-after called CM, of 10 mm in diameter and 16 mm in height, are the starting materials used in this work. From these monoliths, two derived monoliths were prepared. The monoliths, so-called $CM-N_2$, were obtained by heating CM under N_2 flow (100 ml min^{-1}) at 800 ºC for 3 h. The monoliths, so-called CM-48, were obtained by activation under CO_2 flow (100 ml min^{-1}) at 800 ºC for 48 h. Details on the preparation procedures are reported elsewhere [42]. The N_2 treatment was applied to decrease the content of surface oxygen groups while keeping the same surface area. The CO_2 treatment was carried out to increase the porosity and hence the surface area while decreasing the content of surface oxygen groups.

Sub-atmospheric N_2 (at 77K) and CO_2 (at 273K) adsorption/desorption isotherms were measured on a Micromeritics ASAP 2020. Prior to the experiments, the samples were outgassed at 250 ºC for at least 5 h. While the N_2 adsorption gives information about the total micropore volume of the samples, the CO_2 adsorption provides information only about the narrow micropore volumes, i.e. the volume

5

adsorbed in micropores of size < 0.7 nm. Apparent surface areas were obtained from the methods: Brunauer-Emmett-Teller (S_{BET}), Dubinin-Raduskevich (S_{DR}), α-plot ($S_{α-plot}$), t-plot (S_{t-plot}) and Non-Local Density Functional Theory NLDFT (S_{DFT}). From NLDFT, the pore size distributions (PSD) as well as the surface areas due to micropores with sizes above a certain value were obtained.

Temperature-programmed desorption (TPD) experiments were carried out to characterize the surface chemistry of the monoliths. Details on the experimental procedures are reported elsewhere [42]. The intensities of the CO and CO_2 signal were measured to quantify the CO and CO_2 evolved from the monoliths.

The microstructural characterization was carried out by Scanning Electron Microscopy (SEM). Images were obtained in the secondary electron mode by a Jeol JSM 6500 F instrument.

The above mentioned cylindrical monoliths, of 10 mm in diameter and 16 mm in height, were cut in slices of the same diameter and 1.3-1.6 mm in height. These slices, of 0.11-0.14 g in weight, were used as working electrodes in three-electrode cells. Hg/Hg_2SO_4 and platinum wire were the reference electrode and counter electrode, respectively. Aqueous 2M H_2SO_4 solution was chosen as the electrolyte. Prior to the electrochemical measurements, the electrolyte was allowed to infiltrate the monolith for 1.5 days under primary vacuum (ca.10^{-1} Torr).

3. Results and discussion.

3.1 Physical characterization.

A picture of the starting CM monolith is shown in Figure 1a. It is a disk of 10 mm in diameter and 1.3 mm in height. The other monoliths, CM-N_2 and CM-48, show similar looks and sizes (not shown). The SEM image of a fracture of CM shows spheres of ca. 200 μm in diameter that are linked and show not borders between

6

adjacent spheres (arrow-marked in Figure 1b). The spheres or balls are made from carbon particles of ca. 10 µm size; the particles are also linked among them (Figure 1c). The same microstructure is observed for the monoliths CM-N_2 and CM-48 (not shown). The good connectivity between adjacent particles and spheres accounts for the high electrical conductivity found for the three monoliths: 9.3, 9.1 and 9.5 S cm^{-1} for CM, CM-N_2 and CM-48, respectively [42]. These values are among the highest reported for carbon monoliths, usually in the range 1-10 S cm^{-1} and even less [21,24,26,30,31]. The similar conductivities found for the three monoliths show that heating at 800 ºC under N_2 or under CO_2 does not change appreciably the monolith electrical conductivity. Between the adjacent particles and adjacent spheres appear voids of ca. 6 and 50 µm-size, respectively. The two types of voids are connected permitting the entrance of the electrolyte to the spheres and then, to the carbon particles. Therefore, from the electrochemical point of view the three monoliths show two networks: (i) an electronic network made from linked carbon particles and spheres that allows an ease polarization of the double layer as a consequence of the high electrical conductivity and (ii) an ionic network made from connected voids that is filled by the electrolyte ions; this network allows formation of the double layer and redox reactions with oxygen groups of the carbon particles.

The closely compacted microstructure accounts for the high density of the three monoliths: 1.17, 1.03 and 0.80 g cm^{-3} for CM, CM-N_2 and CM-48, respectively. The monolith density decreases with removal of oxygen groups and development of porosity [42]. The density found for the three monoliths is higher than that reported for other carbon monoliths, with densities usually below 0.6 g cm^{-3} [2,20,21,24,26,27,29-32], and also higher than the density of pellets obtained from PVDC-based carbon powders [43,44].

The three monoliths showed I-type N_2 adsorption isotherm (Figure S1 in Supplementary data), which is characteristic of a microporous solid. From the DFT

7

pore size distributions and the close volumes obtained from N_2 and CO_2 adsorption isotherms, it was deduced that most of the micropores had sizes below 0.7 nm in the three monoliths. Only a small portion of the micropores are larger, with sizes up to 1.3 nm [42]. The PSD of CM and CM-N_2 was nearly the same, pointing out that the heating at 800 °C under N_2 flow does not change the size of the pores. This treatment did not appreciably change the specific surface area as measured by different methods: S_{BET}, S_{DR}, $S_{\alpha\text{-plot}}$, $S_{t\text{-plot}}$ and S_{DFT}. In contrast, the CM-48 showed a PSD with higher portion of the micropores larger than 1 nm and also larger specific surface area, the latter being independent on the method chosen [42]. From the DFT method, the total surface area as well as the surface areas associated with micropores larger than a certain value can be estimated. In the literature, sizes for dehydrated and hydrated sulfate ions, of ca. 0.5 nm and 0.6-1 nm, respectively, have been reported [30,43,45-47]. The proton size is still uncertain and the size seems to depend on the pH and counter ion [48-50]. To check how the S_{DFT} surface area changes in relation to the size of the micropores, the sizes above 0.6, 0.75 and 1 nm were arbitrarily chosen and the S_{DFT} values obtained for the three monoliths are shown in Table 1. In the three cases, the main contribution to S_{DFT} is due to micropores smaller than 0.75nm, micropores bigger than 0.75 nm contribute to S_{DFT} with a percentage in the range 9-27 % for the three monoliths. When we pass from CM to CM-N_2, the S_{DFT} due to micropore >0.6 and >0.75 nm increases slightly but S_{DFT} due to micropore sizes >1 nm remains constant. Overall, S_{DFT} increases slightly. When we pass from CM-N_2 to CM-48, the S_{DFT} due to micropores >0.6, >0.75 and > 1 nm increases clearly, especially for micropores >1nm because these micropores are broadened by the activation treatment. Overall, S_{DFT} increases clearly.

Regarding the oxygen functionalities that evolved as CO and CO_2 in TPD, it was shown that the CO and CO_2 content of CM-N_2 and CM-48 are lower than those of CM, i.e. the oxygen functionalities are removed by heating at 800 °C either under N_2 flow for

8

3 h or under CO_2 flow for 48 h, the removal being more important for the latter

treatment that was applied for longer time [42]. Because the CO contents are taken

below to estimate the pseudocapacitance, those contents are collected in Table 3 for

the three monoliths.

3.2 Electrochemical study in three-electrode cells.

In a previous work some of us reported a gravimetric and volumetric

capacitance as high as 292 F g^{-1} and 342 F cm^{-3}, respectively, for the starting CM

monolith in acidic electrolyte [42]. These values, which are the highest ever reported in

acidic electrolyte, were measured in two-electrode cells, and hence the capacitances

are due to the contribution of the two types of ions, sulfate ions and protons. In this

work, the capacitance due to each type of ion is measured and its contribution to the

total capacitance as well as to the double layer capacitance is discussed. The

galvanostatic measurements were carried out at low current density (1 mA cm^{-2}) to get

electrochemical responses in nearly steady-state conditions, i.e. not affected by kinetic

effects. The galvanostatic plots in the voltage range from -0.6 to 0.4 V vs. Hg/Hg_2SO_4,

which is nearly the same voltage range from 0 to 1V vs. SHE, are shown in Figure 2.

Between the open circuit voltage (OCV) and positive voltages vs. Hg/Hg_2SO_4, the

sulfate ions are electroadsorbed and electrodesorbed. Between the OCV and negative

voltages vs. Hg/Hg_2SO_4, the protons are electroadsobed and electrodesorbed, may be

together with reversible redox reactions as discussed below. Therefore, during the

complete discharge and complete charge, both in the voltage range from -0.6 to 0.4 V

vs. Hg/Hg_2SO_4 or from 0 to 1V vs. SHE, the sulfate ions and protons are involved.

During the discharge, the sulfate ions are desorbed and the protons are adsorbed, may

be together with reversible reduction reactions. The reverse happens during the charge

in which protons are desorbed, may be together with oxidation reactions, and sulfate

ions are adsorbed.

9

As the upper positive voltage increases from 0.25 to 0.4 V vs. Hg/Hg_2SO_4 (see the third cycle in Figure 2), the shape of the plot becomes progressively distorted, showing a new regime of lower slope. This regime, which appears at voltages close to 1 V vs. SHE, can be ascribed to oxygen evolution associated with water decomposition. The presence of this regime does not affect the capacitance measured during the discharge between the upper positive voltage and -0.6 V. Indeed, the capacitance was nearly the same, 36-38 F, for the three cycles (see the blue straight lines in Figure 2). The specific capacitance during the total discharge was determined according to C_{1s} total$=I \cdot t_d/E_2 \cdot m$; where I is the current applied, t_d is the discharge time between the upper voltage (0.25 V) and -0.6 V, E_2 is the voltage range during the discharge, and m is the monolith mass. The values of C_{1s} total are close to those of the specific capacitance, C_{1s} 2E, measured in a two-electrode cell [42] (see Table 2).

The specific capacitance, due separately to the sulfate ions and protons, was determined by galvanostatic measurements, also at 1 mA cm^{-2}, in the voltage range from OCV to 0.25 V (sulfate ions) and from OCV to -0.6 V (protons). These measurements are plotted as an example for the CM monolith in Figure 3. The specific capacitance C_{1s} due to sulfate ions and protons was determined according to the expression $I \cdot t/E \cdot m$; where I is the current applied, t is the time during charge or discharge, E is the voltage range during charge or discharge, and m is the monolith mass. For the three monoliths, the values of C_{1s} obtained on charge (electroadsorption) are close to those obtained on discharge (electrodesorption); the average of the two values is taken as the representative specific capacitance of the sulfate ions (C_{1s} SO_4^{2-}) and protons (C_{1s} H^+) in each monolith (Table 2). C_{1s} SO_4^{2-} is much lower than C_{1s} H^+ for CM, slightly lower for $CM-N_2$, and nearly the same for CM-48. Comparing the values obtained for the three monoliths, C_{1s} SO_4^{2-} increases along the series CM<$CM-N_2$<CM-48. The trend agrees with the progressive increase of the specific surface area (Table 1) and indicates a main contribution of the double layer capacitance to the C_{1s} SO_4^{2-}

measured; hence, C_{1s} SO_4^{2-} = C_{1s} (DL) SO_4^{2-}. In contrast, C_{1s} H$^+$ decreases from CM to

CM-N$_2$ but increases from CM-N$_2$ to CM-48. This trend suggests the presence of two

contributions for C_{1s} H$^+$: a double layer capacitance, C_{1s}(DL) H$^+$, and a

pseudocapacitance, C_{1s}(PS) H$^+$. To check the possible presence of a

pseudocapacitance in addition to double layer capacitance, cyclic voltammetries were

recorded for the sulfate ions and protons on the three monoliths. As representative

examples, the cyclic voltammetries obtained for CM and CM-48 are shown in Figure 4.

These monoliths were chosen because they show the highest and lowest content in

oxygen groups (Table 3). For the two monoliths, the voltammogram ascribed to the

sulfate ions shows a rectangular shape, which is characteristic of the double layer

capacitance. It supports again that C_{1s} SO_4^{2-}= C_{1s} (DL) SO_4^{2-}. However, the

voltammograms due to the protons show broad peaks or humps at ca. -0.1 and -0.25

V, revealing the presence of pseudocapacitance in addition to the double layer

capacitance. Hence, C_{1s} H$^+$=C_{1s}(DL) H$^+$ + C_{1s}(PS) H$^+$. The presence of a

pseudocapacitance has been found in aqueous electrolytes, such as sulfuric acid and

potassium hydroxide, for carbons having several oxygen groups (ketone, carboxylic

acid, anhydrides, etc.) [51-61]. Estimation of the pseudocapacitance and separation of

the pseudocapacitance from the double layer capacitance has been made on the basis

of the linear dependence found between pseudocapacitance and CO-generating

oxygen groups, despite different oxygen groups seem to be involved [58,60]. Taking

into account that the monoliths studied in this work are microporous, the

pseudopcapacitance has been assessed according to the methodology reported for

microporous carbons. The pseudocapacitance was found to be proportional to the

content of CO-evolving groups with a rate of 0.063±0.005 F μmol^{-1} of CO for

microporous bead carbons [58] and with a rate of 0.042±0.008 F μmol^{-1} of CO for

micropourous carbon nanofibers [60]. The two values are close within experimental

error. Because our microporous carbon monoliths are made from carbon microbeads

11

as deduced from the SEM study, the pseudocapacitance $C_{1s}(PS)$ H$^+$ for each monolith was estimated according to the equation:

$$C_{1s}(PS) \text{ H}^+ = (0.063 \text{ F } \mu mol^{-1} \text{ of CO}) \times (CO \text{ content}) \qquad (1)$$

where the CO *content* expressed in µmol CO g^{-1} is the amount of CO evolved in TPD experiments (Table 3). Then, $C_{1s}(DL)$ H$^+$ was calculated as $C_{1s}(DL)$ H$^+$ = C_{1s}H$^+$ - $C_{1s}(PS)$ H$^+$. Table 3 outlines the double layer capacitance obtained for the two types of ions, C_{1s} (DL) SO$_4^{2-}$ and $C_{1s}(DL)$ H$^+$, and the pseudocapacitance obtained for the protons, $C_{1s}(PS)$ H$^+$. As expected, $C_{1s}(PS)$ H$^+$ decreases along the series CM>CM-N$_2$>CM-48 in agreement with the progressive decrease in the content of oxygen functionalities. In contrast, $C_{1s}(DL)$ H$^+$ increases progressively according to CM≈CM-N$_2$<CM-48; it agrees with the increase in specific surface area from CM to CM-48. Therefore, the anomalous variation observed for C_{1s} H$^+$ along the series CM, CM-N$_2$, CM-48 (Table 2) is a consequence of the presence of two contributions, $C_{1s}(PS)$ H$^+$ and $C_{1s}(DL)$ H$^+$.

Comparing the values of $C_{1s}(DL)$ SO$_4^{2-}$ with those of $C_{1s}(DL)$ H$^+$ for the three monoliths, $C_{1s}(DL)$ SO$_4^{2-}$ is slightly higher (1.2-1.4 times) than $C_{1s}(DL)$ H$^+$ (Table 3). This result could suggest a preference of the sulfate ions against protons to form the double layer. However, the fact that $C_{1s}(DL)$ SO$_4^{2-}$/$C_{1s}(DL)$ H$^+$ ratio is below 2, while the charge of the sulfate ions is 2 and the charge of the protons is 1, indicates that the higher value of $C_{1s}(DL)$ SO$_4^{2-}$ compared to $C_{1s}(DL)$ H$^+$ comes from the higher charge of the sulfate ions and not from a higher amount of these electroadsorbed ions at the double layer. To illustrate this point, the ratio of the amount of the two types of ions that form the double layer for a given voltage, ΔV, can be calculated according to the equation:

$$N \text{ protons}/N \text{ sulfate ions} = [(C_{1s}(DL) \text{ H}^+) \cdot \Delta V]/[(C_{1s}(DL) \text{ SO}_4^{2-}) \cdot \Delta V/2] \qquad (2)$$

where the factor 2 comes from the double charge of the sulfate ions. The ratio of N protons/N sulfate ions is in the range 1.5-1.7 for the three monoliths. Therefore, the

12

monoliths show a preference to electroadsorb protons at the double layer as compared to sulfate ions. Taking into account that the three monoliths are microporous, and that most of the micropores have sizes below 0.75 nm as already discussed, the preference of protons to be electroadsorbed at the double layer points to a smaller size of these ions as compared to the electroadsorbed sulfate ions. However, based on the ratio of the two electroadsorbed ions at the double layer for the same ΔV, it is difficult to guess the sizes of the two electroadsorbed ions.

Taking into account: (i) the double layer capacitance of the sulfate ions and protons as shown in Table 3, and (ii) the short voltage window (0.25 V) at which the sulfate ions are electroadsorbed/electrodesorbed and the longer voltage window (0.6 V and even more) at which protons are electroadsorbed/ electrodesorbed at the double layer, it is possible to estimate the relative contribution of the two types of ions to the capacitance of the double layer. Thus, for a total voltage window of 0.85 V:

$$C_{DL} = [(C_{1s}(DL) \, SO_4^{2-}) \cdot 0.25 + (C_{1s}(DL) \, H^+) \cdot 0.6]/0.85 \qquad (3)$$

the contribution of the sulfate ions and protons to the double layer capacitance is ca. 0.3 and 0.7, respectively, i.e. 30% and 70 % for the three monoliths. The same contributions are found if a total voltage window of 1.1 V is considered, with 0.25 V for the sulfate voltage window and 0.85 V for the proton voltage window. These results provide evidence that protons dominate the capacitance of the double layer in a real two-electrode supercapacitor having microporous carbon monoliths as electrodes.

CONCLUSIONS

The monoliths studied in this work show two networks, one network of connected carbon particles and spheres that provide high electrical conductivity, and another one of connected voids that provide access of the electrolyte ions to the

13

carbon particles. The closely compacted microstructure accounts for the high density of the monoliths. The micropores of the carbon particles, most of them with sizes below 0.75 nm, account for the large surface area of the monoliths, 1000-1600 $m^2 g^{-1}$.

Measurements in three-electrode cells have permitted us to determine separately the specific capacitances due to the sulfate ions and protons. The specific capacitance of the sulfate ions is ascribed to a double layer capacitance only. The specific capacitance of the protons shows a pseudocapacitance in addition to double layer capacitance. The pseudocapacitance decreases along the series CM>CM-N_2>CM-48, i.e. as the content in surface oxygen groups decreases. The double layer capacitance due to the sulfate ions and protons increases slightly from CM to CM-N_2 and more pronounced to CM-48, i.e. as the specific surface area increases. Although the double layer capacitance due to the sulfate ions is slightly higher than that due to protons in the three monoliths, the larger voltage window of protons compared to sulfate ions makes the contribution of protons to the capacitance of the double layer much higher (ca. 70 %) than that of sulfate ions (ca. 30 %). For a given voltage, the number of protons forming the double layer is higher (1.5-1.7 times) than that of sulfate ions. It indicates a preference of protons to be electroadsorbed at the double layer that seems to be associated with the microporous feature of the carbon monoliths.

Acknowledgements

REFERENCES

[1] R. Saliger, U. Fischer, C. Herta , J. Fricke, J. Non-Cryst. Solids 225 (1998) 81.

[2] D. Wu, R. Fu, S. Zhang, M. Dresselhaus, G. Dresselhaus, Carbon 42 (2004) 2033.

[3] J. Biener, M. Stadermann, M. Suss, M. A. Worsley, M.M. Biener, K.A. Rose, T.F. Baumann, Energy Environ. Sci. 5 (2011) 656.

[4] N. Brun, S.R.S. Prabaharan, C. Surcin, M. Morcrette, H. Deleuze, M. Birot, O. Babot, M.F. Achard, R. Backov, J. Phys. Chem. C116 (2012) 1408.

[5] S.L. Candelaria, R. Chen, Y.-H.Jeong, G. Cao, Energy Environ. Sci., 5 (2012) 5619.

[6] A. Garcia-Gomez, P. Miles, T.A. Centeno, J.M. Rojo, Electrochem. Solid-State Lett.13(8) (2010) A112.

[7] H. Yang, Q. Shi, X. Liu, S. Xie, D. Jiang, F.Zhang, C. Yu, B. Tu, D. Zhao, Chem. Commun. (2002) 2842.

[8] J.-S. Yu, S. Kang, S.B. Yoon, G. Chai, J. Am. Chem. Soc. 124 (2002) 9382.

[9] A. Taguchi, J.H. Smatt, M. Linden, Adv. Mater. 15 (2003) 1209.

[10] T.F. Baumann, J.H. SatcherJr, J. Non-Cryst. Solids 350 (2004) 120.

[11] N. Tonanon, A. Siyasukh, Y. Wareenin, T. Charinpanitkul, H. Nishihara, S.R. Mukai, H. Tamon, Carbon 43 (2005) 2808.

[12] S.R. Mukai, H. Nishihara, T. Yoshida, K. Taniguchi, H. Tamon, Carbon 43 (2005) 1557.

[13] Z. Zhou, Q. Yan, F. Su, X.S. Zhao, J. Mater. Chem. 15 (2005) 2569.

[14] N. Liu, S. Zhang, R. Fu, M.S. Dresselhaus, G. Dresselhaus, J. Appl. Polymer Sci. 104 (2007) 2849.

[15] J. Li, X. Wang, Y. Wang, Q. Huang, C. Dai, S. Gamboa and P.J. Sebastian, J. Non-Cryst. Solids 354 (2008) 19.

[16] S. Xu, J. Li, G. Qiao, H. Wang, T. Lu, Carbon 47 (2009) 2103.

[17] M. Sevilla, A.B. Fuertes, Carbon 56 (2013) 155.

[18] S.J. Kim, S.W. Hwang, S.H. Hyun, J. Mater. Sci. 40 (2005) 725.

[19] B. Batalla Garcia, A.M. Feaver, Q. Zhang, R.D. Champion, G. Cao, T.T. Fister, K.P. Nagle and G.T. Seidler, J. App. Phys. 104 (2008) 014305.

[20] V. Ruiz, C. Blanco, R. Santamaria, J.M. Ramos-Fernandez, M. Martinez-Escandell, A. Sepulveda-Escribano, F. Rodriguez-Reinoso, Carbon 47 (2009) 195.

[21] A. Garcia-Gomez, P. Miles, T.A. Centeno, J.M. Rojo, Electrochim. Acta 55 (2010) 8539.

[22] J. Chmiola, C. Largeot, P.L. Taberna, P. Simon and Y. Gogotsi, Science 328 (2010) 480.

[23] M.M. Bruno, N.G. Cotella, M.C. Miras, C.A. Barbero, Colloids Surfaces A: Physicochem. Eng. Aspects 362 (2010) 28.

[24] D. Carriazo, F. Pico, M.C. Gutierrez, F. Rubio, J.M. Rojo and F del Monte, J. Mater. Chem. 20 (2010) 773.

[25] A. Halama, B. Szubzda, G. Pasciak, Electrochim. Acta 55 (2010) 7501.

[26] E. Taer, M. Deraman, I.A. Talib, A. Awitdrus, S.A. Hashmi, A.A. Umar, Int. J. Electrochem. Sci. 6 (2011) 3301.

[27] A. Awitdrus, M. Deraman, I.A. Talib, R. Farma, R. Omar, M.M. Ishak, N.H. Basri and B.N.M. Dolah, Adv. Mater. Research 501 (2012) 13.

[28] M.-C. Liu, L.-B.Kong, P. Zhang, Y.-C.Luo, L. Kang, Electrochim. Acta 60 (2012) 443.

[29] P. Staiti, A. Arenillas, F. Lufrano, J.A. Menendez, J. Power Sources 214 (2012) 137.

[30] G. Hasegawa, K. Kanamori, K. Nakanishi, T. Abe, J. Phys. Chem. C 116 (2012) 26197.

[31] M. Zeller, V. Lorrmann, G. Reichenauer, M. Wiener, J. Pflaum, Adv. Energy Mater. 2 (2012) 598.

[32] P.A. Goodman, H. Li, Y. Gao, Y.F. Lu, J.D. Stenger-Smith, J. Redepenning, Carbon 55 (2013) 291.

[33] S.H. Lee, H.W. Kim, J.O. Hwang, W.J. Lee, J. Kwon, C.W. Bielawski, R.S. Ruoff, S.O. Kim, Angew. Chem. Int. Ed. 49 (2010) 10084.

[34] G. Hasegawa, M. Aoki, K. Kanamori, K. Nakanishi, T. Hanada, K. Tadanaga, J. Mater. Chem. 21 (2011) 2060.

[35] D. Carriazo, M.C. Gutierrez, F. Pico, J.M. Rojo, J.L.G. Fierro, M.L. Ferrer, F. del Monte, Chem. Sus. Chem. 5 (2012) 1405.

[36] D.-W. Wang, F. Li, L.-C. Ying, X. Lu, Z.-G.Chen, I.R. Gentle, G.Q. Lu, H.-M. Cheng, Chem. Eur. J. 18 (2012) 5345.

[37] X. Zhao, Q. Zang, C.-M. Chen, B. Zhang, S. Reiche, A. Wang, T. Zhang, R. Schlogl, D.S. Su, Nano Energy 1 (2012) 624.

[38] U.N. Maiti, W.J. Lee, J.M. Lee, Y. Oh, J.Y. Kim, J.E. Kim, J. Shim, T.H. Han, S.O. Kim, Adv. Mater. 26 (2014) 40.

[39] L.-Z. Fan, Y.-S. Hu, J. Maier, Ph. Adelhelm, B. Smarsly, M. Antonietti, Adv. Funct. Mater.17 (2007) 3083.

[40] J.M. Miller, B. Dunn, T.D. Tran, R.W. Pekala, J. Electrochem Soc. 144(12) (1997) L309.

[41] G.-R. Li, Z.-P.Feng, Y.-N.Ou, D. Wu, R. Fu, Y.X. Tong, Langmuir 26(4) (2010) 2209.

[42] M. Kunowsky, A. Garcia-Gomez, V. Barranco, J.M. Rojo, J. Ibañez, J.D. Carruthers, A. Linares-Solano, Carbon 68 (2014) 553.

[43] M. Endo, Y.J. Kim, T. Takeda, T. Maeda, T. Hayashi, K. Koshiba, H. Hara, M.S. Dresselhaus, J. Electrochem. Soc. 148(19) (2001) A1135.

16

[44] B. Xu, F. Wu, S. Chen, Z. Zhou, G. Cao, Y. Yang, Electrochim. Acta 54 (2009) 2185.

[45] L. Eliad, E. Pollak, N. Levy, G. Salitra, A. Soffer, D. Aurbach, Appl. Phys. A 82 (2006) 607.

[46] V. Vchirawongkwin, B.M. Rode, I. Persson, J. Phys. Chem. B, 111 (2007) 4150.

[47] J. Huang, B.G. Sumpter, V. Meunier, Chem. Eur. J. 14 (2008) 6614.

[48] L.Eliad, G. Salitra, A. Soffer, D. Aurbach, Langmuir 21 (2005) 3198.

[49] R. Heyrovska, Chem. Phys. Lett. 432 (2006) 348.

[50] R. Mancinelli, A. Sodo, F. Bruni, M.A. Ricci ,A.K. Soper, J. Phys. Chem. B, 113 (2009) 4075.

[51] Y.R. Nian , H. Teng, J. Electrochem. Soc., 149(8) (2002) A1008.

[52] M.J. Bleda-Martinez, J.A. Macia-Agullo, D. Lozano-Castello, D. Cazorla-Amoros, and A. Linares-Solano, Carbon 43 (2005) 2677.

[53] K. Okajima, K. Ohta, M. Sudoh, Electrochim. Acta 50 (2005) 2227.

[54] F.-C. Wu, R.-L. Tseng, C.-C. Hu, C.-C. Wang, J. Power Sources 144 (2005) 302.

[55] H.A. Andreas and B. Conway, Electrochim. Acta51 (2006) 6510.

[56] E. Raymundo-Piñero, F. Leroux, F. Beguin, Adv. Mater. 18 (2006) 1877.

[57] C.-C. Hu, J.-H. Su, T.C. Wen, J. Phys. Chem. Solids 68 (2007) 2353.

[58] T.A. Centeno, M. Hahn, J.A. Fernandez, R. Kotz, F. Stoeckli, Electrochem. Comun. 9 (2007) 1242.

[59] Q. Bao, S. Bao, C.M. Li, X. Qi, C. Pan, J. Zhang, Z. Lu, Y. Li, D.Y. Tang, S. Zhang, K . Lian, J. Phys. Chem. C 112 (2008) 3612.

[60] V. Barranco, M.A. Lillo-Rodenas, A. Linares-Solano, A. Oya, F. Pico, J. Ibañez, F. Agullo-Rueda, J.M. Amarilla, J.M. Rojo, J. Phys. Chem. C 114 (2010) 10302.

[61] Carbons for electrochemical energy storage and conversion systems. Ed. F. Beguin and E. Frackowiak. Chapter 5. CRC Press, Taylor and Francis Group, 2010.

17

FIGURE CAPTIONS

Figure 1.-Picture of the starting CM monolith used as electrode (a). SEM image obtained on the cross-section fracture of the monolith (b), and a magnification showing the spheres, carbon particles and voids (c).

Figure 2.-Galvanostatic plot obtained in a three-electrode cell on the CM monolith. The current density applied was 1 mA cm^{-2}.

Figure 3.-Partial galvanostatic plots obtained for sulfate ions (a) and protons (b) on the CM monolith in a three-electrode cell. The current density applied was 1 mA cm^{-2}.

Figure 4.-Cyclic voltammetries (blue circles) obtained on the CM and CM-48 monolith in a three-electrode cell. The partial cyclic voltammetries due to sulfate ions and protons are also shown. The voltage scan rate was 0.1 mV s^{-1} in all cases.

Table 1. Specific surface area (in $m^2 \, g^{-1}$ and percentage) estimated for all micropores and for micropores bigger than 0.6, 0.75 and 1 nm from N_2-DFT.

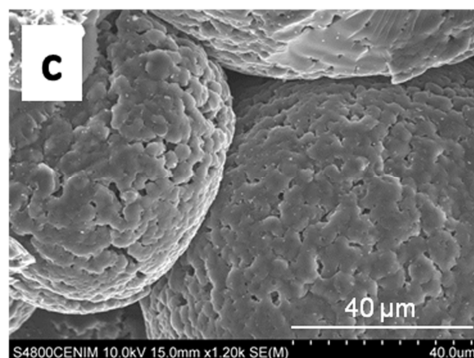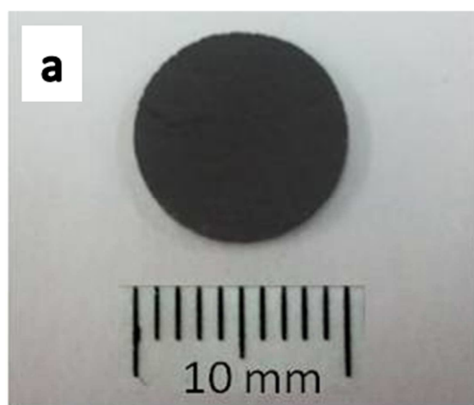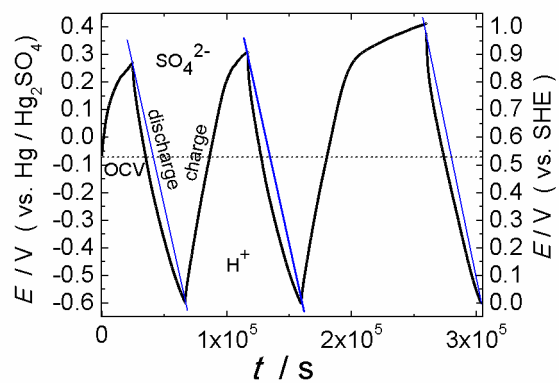| Micropore size	CM		CM-N_2		CM-48	
	($m^2 \, g^{-1}$)	(%)	($m^2 \, g^{-1}$)	(%)	($m^2 \, g^{-1}$)	(%)
all	966	100	1067	100	1625	100
>0.6 nm	267	28	314	29	835	51
>0.75 nm	157	16	183	17	569	35
>1 nm	104	11	92	9	432	27

Table 2. Specific capacitance (C_{1s}) measured from the electroadsorption (ads) and electrodesorption (des) of the sulfate ions and protons in partial galvanostatic plots. Average values of C_{1s} for both ions are $C_{1s}SO_4^{2-}$ and $C_{1s}H^+$. Total specific capacitance (C_{1s} total) was measured in the voltage range from 0.25 to -0.6 V. All measurements were carried out at 1 mA cm^{-2} in a three-electrode cell. For comparison, the values of C_{1s} obtained at the same current density in two-electrode cell (C_{1s} 2E) are included [42].

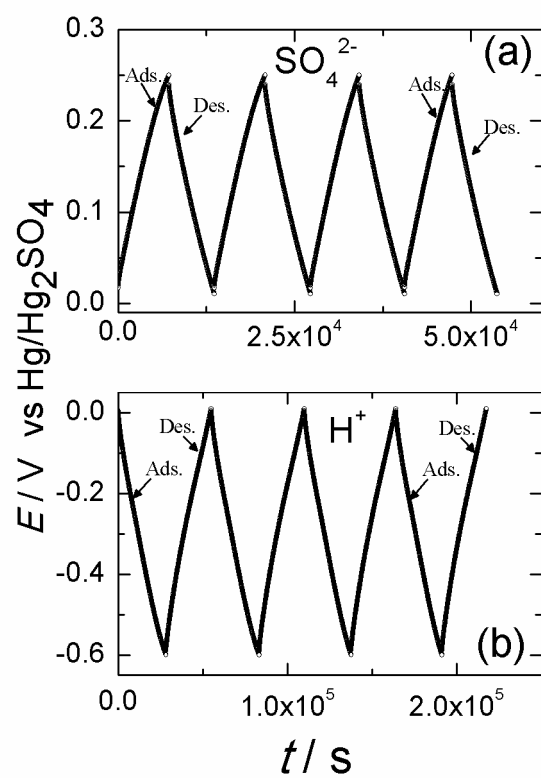| Monolith	SO_4^{2-} ads C_{1s} (F g^{-1})	SO_4^{2-} des C_{1s} (F g^{-1})	H^+ ads C_{1s} (F g^{-1})	H^+ des C_{1s} (F g^{-1})	$C_{1s}SO_4^{2-}$ (F g^{-1})	$C_{1s}H^+$ (F g^{-1})	C_{1s} total (F g^{-1})	C_{1s} 2E (F g^{-1})
CM	199	193	326	313	196	320	287	292
CM-N$_2$	232	210	249	248	221	248	247	241
CM-48	294	288	290	282	291	286	287	291

Table 3. Specific double layer capacitance ascribed to the sulfate ions ($C_{1s}(DL)$ SO_4^{2-}) and protons ($C_{1s}(DL)$ H^+), and specific pseudocapacitance ascribed to the protons ($C_{1s}(PS)$ H^+). The CO contents deduced from TPD measurements are also included.
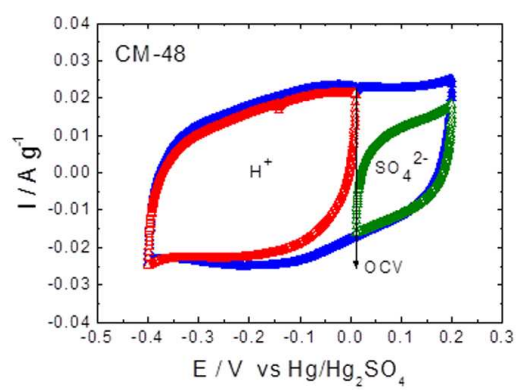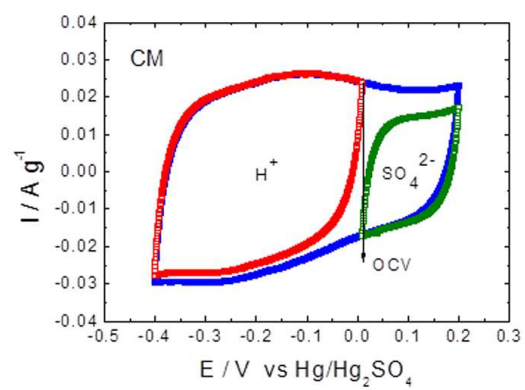
Monolith	CO content (μmol g^{-1})	$C_{1s}(PS)$ H^+ (F g^{-1})	$C_{1s}(DL)$ H^+ (F g^{-1})	$C_{1s}(DL)$ SO_4^{2-} (F g^{-1})
CM	2411	152	168	196
CM-N$_2$	1314	83	165	221
CM-48	552	35	251	291

HIGHLIGHTS

The specific capacitance of microporous carbon monoliths in sulfuric acid is studied

The double layer capacitance of sulfate ions is higher than that of protons

At the double layer, the amount of electroadosrbed protons is higher than sulfates

Protons dominate the double layer capacitance of the microporous monoliths

Protons also contribute with a pseudo capacitance which is assessed

SUPPLEMENTARY DATA OF THE ARTICLE

The contribution of sulfate ions and protons to the specific capacitance of microporous carbon monoliths.

by

V. Barranco[1], A. Garcia-Gomez[1], M. Kunowsky[2], A. Linares-Solano[2], J. Ibañez[3], M. King[4], and J.M. Rojo[1]*

1. Instituto de Ciencia de Materiales de Madrid, ICMM; CSIC; Sor Juana Ines de la Cruz, 3; Cantoblanco; 28049-Madrid; Spain.

2. Grupo MCMA; Departamento de Quimica Inorganica; Universidad de Alicante; Ap. 99; 03080-Alicante; Spain.

3. Centro Nacional de Investigaciones Metalurgicas, CENIM; CSIC; 28040-Madrid; Spain

4. ATMI, Adsorbent and Gas Technology; Danbury; Connecticut 06810; USA.
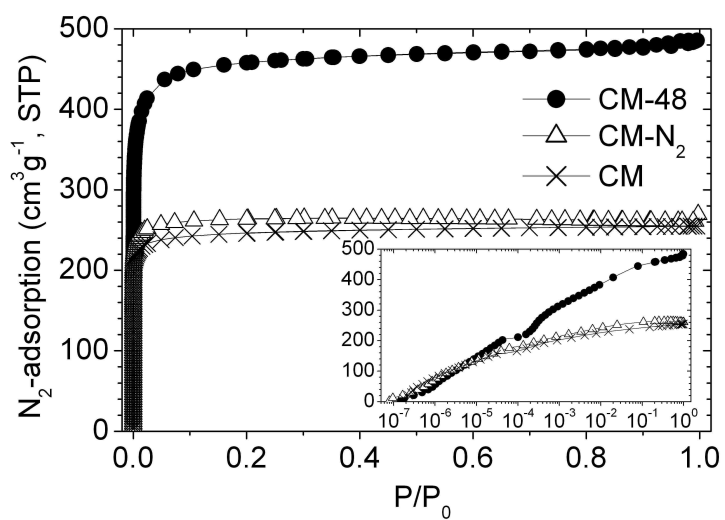
*corresponding author: jmrojo@icmm.csic.es

Figure S1. Nitrogen adsorption isotherms recorded on the monoliths CM, CM-N$_2$ and CM-48. The inset shows the isotherms plotted in a logarithmic scale on the relative pressure axis.